# Theoretical Investigations of a Proposed Series Integration of Resonant Tunneling Diodes for Millimeter-Wave Power Generation

Cheng Chih Yang, *Member, IEEE,* and Dee-Son Pan, *Member, IEEE*

*Abstract*—**Double-barrier quantum-well resonant tunneling diode (RTD) has great potential for power generation at millimeter-wave frequencies. If a number of RTD's are integrated in series, the integrated device can greatly increase the total output power and help remove the problem of low-frequency spurious oscillations associated with a single RTD. The feasibility of such a proposed series integration scheme is investigated. The advanced monolithic nonlinear transmission line (NLTL) generating picosecond voltage shock waves can be used to initiate oscillation in such series-integrated RTD's to overcome the dc instability. The large-signal RF characteristics of the series-integrated RTD's are analyzed and simulated, including transit time effects in the depletion region. Using one of the available GaAs/AlAs RTD data, our computer simulation results show that a total cw output power of about 0.1 W with a dc-to-RF conversion efficiency of about 8% can be generated to a 5-Ω load at 100 GHz, if ten such RTD's are integrated in series.**

## I. Introduction

DOUBLE-BARRIER quantum-well resonant tunneling diode (RTD) has recently attracted considerable attention due to its potential applications in both RF and digital areas [1], [2]. The diode structure is composed of a thin quantum-well layer sandwiched by two very thin barrier layers. The current first increases monotonically with the bias voltage. The peak current occurs when the energy of most of the incident electrons is in resonance with the energy levels in the well. The current then drops after the resonance is passed. A negative differential resistance (NDR) is therefore displayed on the diode dc current-voltage ($I$–$V$) characteristics. This intrinsic NDR is potentially useful for power generations at millimeter-wave frequencies. For example, Brown *et al.* [1] reported that 18 $\mu$W output power from a RTD fabricated by GaAs/AlAs double-barrier quantum-well structure was measured at a second harmonic oscillation frequency of 87 GHz. More recently, oscillations up to 420 GHz with 0.2 $\mu$W from the same kind of diode were observed [3]. It has been pointed out that the depletion region adjacent to the double-barrier quantum well is useful for the RTD RF performance [4], [5]. Experimental progresses were further made by Kesan *et al.* [6] and Grönqvist *et al.* [7] with a more detailed consideration of transit time effects in the depletion region. RTD's have also been fabricated in other material system, such as $In_{0.53}Ga_{0.47}As/As/InAs$ and InAs/AlSb, to achieve high current density, low peak voltage, and large peak-to-valley current ratio.

Generally speaking, both RTD and tunnel diode utilize tunneling mechanism for generating current; one uses barrier resonant tunneling and the other interband tunneling. The intrinsic frequency response for both tunneling processes is very high, i.e., in the THz range. Due to limited density of states in the bands, peak current density in both cases is limited to about $10^5$ A/cm$^2$. Higher cutoff frequency requires large peak current density and smaller capacitance. The RTD produces a higher cutoff frequency than the tunnel diode due to its lower capacitance resulting from the added adjacent region. This added depletion region is impossible for a tunnel diode. Simple estimates indicate the RTD's can be operated at millimeter-wave frequencies while tunnel diodes can not. From device point of view, the utilization of the depletion region is crucial to high cutoff frequency. The inclusion of the depletion region in a RTD requires consideration of transit time effects. The transit time effects have been analyzed by Kesan *et al.* [4], and Song and Pan [5]. In this paper, transit time effects are included in our analysis.

The power generated from a single RTD as reported in [1], [3], [6], and [7] is too small for many practical applications. In principle, more diodes can be connected in series to increase the total output power [8], [9]. It can be achieved by utilizing modern fabrication technology such as MBE (molecular beam epitaxy) to grow a number of RTD's in series on the same wafer [2], [10]. Ohmic loss can thus be minimized by making intimate device-level integration. However, it is known that oscillation can not be triggered in a circuit consisting of series-connected NDR diodes unless the dc power supply is turned on fast enough [8]. Normally, a circuit consisting of series-connected NDR diodes is dc unstable when all of them are biased in the NDR regime. Nevertheless, when a turn-on process is so fast that the capacitive current dominates, the initial distribution of the total voltage can be equally

Manuscript received November 20, 1990; revised September 25, 1991.

C. C. Yang is with the Electronic Systems Group, TRW, Inc., One Space Park, Redondo Beach, CA 90278.

D.-S. Pan is with the Electrical Engineering Department, University of California, Los Angeles, Los Angeles, CA 90024.

IEEE Log Number 9105451.

partitioned among individual NDR diodes and be controlled to reach into NDR regime of each diode $I$–$V$ characteristics [8]. In this way, RF oscillation can be initiated. The oscillation can be maintained if a proper embedding circuit is designed [8]. Such an oscillation process in a circuit made of series-connected tunnel diodes was experimentally demonstrated by Vorontsov and Polyakov [8]. For a millimeter-wave frequency implementation of this scheme with series-integrated RTD's, an extremely fast switch to turn on a dc power supply in about a picosecond is required. Fortunately, this can be accomplished by the recently developed nonlinear transmission line (NLTL) technique [11]. It has been reported that 6-V amplitude shock waves with 1.6-ps fall times can be generated by a GaAs monolithic NLTL periodically loaded with hyperabrupt-doped Schottky diodes [11]. Therefore, the oscillation scheme described in [8] is possible at millimeter-wave frequencies with present technology.

There is another potential advantage of such series-integration of RTD's. It is generally noticed that low-frequency spurious oscillations are associated with a single RTD operation because of its high NDR at low frequencies. This makes millimeter-wave RTD oscillator design very difficult. If two or more NDR diodes are connected in series in the proposed scheme, stable self-oscillation occurs only within a narrow frequency band [8]. Therefore, the undesirable low-frequency oscillations can be eliminated once an appropriate circuit design is carried out to initiate and maintain oscillation. Of course, the design for such an appropriate circuit may not be simple, either. This still needs to be investigated.

In this paper, we will analyze in detail the feasibility and the performance of millimeter-wave oscillations of series-integrated RTD's from the device operation point of view. In next section, a structure of series-integrated RTD's will be proposed. The design is mainly based on the dc characteristics and qualitative RF analysis of a single RTD. The quantitative formulations for RF steady-state analysis of the proposed structure are presented in Section III, where transit time effects are treated. As will be shown, transit time effects will not invalidate the oscillation scheme. Following the approach in Section III, simulation results are presented in Section IV. Finally, the overall performance of series-integrated RTD's are discussed in Section V. We conclude that the power enhancement by series-integrated RTD's is very attractive for future millimeter-wave power source.

## II. Design Considerations of the Proposed Device

In attempts to increase the battery efficiency by utilizing tunnel diodes, Vorontsov and Polyakov [8] had analyzed and experimentally verified an oscillatory process in circuits with several series-connected tunnel diodes. An oscillator with as many as ten tunnel diodes connected in series had been demonstrated [8]. In order to initiate self-oscillation for series-integrated NDR diodes, the turn-on time of the dc bias voltage must be short enough. If all the diodes are assumed identical, the turn-on time should be shorter than the transient time of the dc instability. The transient time in this case is determined by the negative resistance in NDR regime, the diode capacitance, and the initial current or voltage spread between diodes in the series-integrated structure. Practically, each individual diode can not be identical, so the difference of the diode $I$–$V$ characteristics can dominate the transient of the dc instability as was found in [8]. For tunnel diodes, the spread in peak currents was identified as the crucial parameter to determine dc instability. The spread of the peak currents in the integrated RTD's is expected. The peak current of a RTD is primarily controlled by barrier thickness, which is very thin ($\leq 15$ Å) and critical to grow. It is also possible to find a spread in peak voltages. The peak voltage of a RTD is essentially determined by the quantum well thickness and the depletion region thickness, which are supposedly more controllable than the barrier thickness. It should be noted that for RTD's the $C(V)$ characteristic is much more controllable than the $I(V)$ characteristic in general. This facilitates the self-oscillation initiation in a series-integrated structure by a fast turn-on voltage.

Since the cutoff frequency of the RTD used here is much higher than that of the tunnel diode due to its smaller capacitance, an ultrafast turn-on is needed. Using the experimental data from [1], the minimum slope of the excitation pulse leading edge is estimated to be $5 \times 10^{11}$ V/s according to [8], when ten RTD's are integrated with a 20% spread of peak currents. (Note that the corresponding value estimated in [8] for ten tunnel diodes was about $2 \times 10^{9}$–$2 \times 10^{10}$ V/s). The reported results in [11] indicate that the NLTL is capable of providing such a minimum voltage pulse slope. Therefore, the oscillation process described in [8] is entirely feasible today for series-integrated RTD's if the advanced NLTL technology is used.

The design considerations for the proposed series-integrated device structure of RTD's need to be addressed. To be more specific, we choose GaAs/AlAs material system for an oscillation frequency of 100 GHz as an example. The analysis can be extended straightforwardly to the whole millimeter-wave frequency range and other material systems. Because the frequency is substantially higher than that in [8], many new effects should be considered, namely, distributed circuit effect, skin effect, carrier transit time effects, and transient effects of carrier motions.

First of all, the size of the total integrated device structure is still much smaller than the electromagnetic wavelength of the oscillation frequency, so the lumped-circuit approximation is still valid, i.e., the distributed-circuit consideration is not required. Another aspect about the validity of the lumped-circuit approach to the series-integrated structure is the following. Because the distance between any two adjacent RTD's is very small ($\leq 500$ Å), attention has to be paid that there is no phase coherence for the electron motion from one RTD to its neighbor

RTD's. This has been experimentally verified [10]. Thus, the lumped-circuit description for each individual RTD in the integration structure is fully justified. However, transit time effects in each RTD element, which depend on the carrier transport in the depletion region, turn out to be not negligible. Although accurate simulation should include transit time effects, a simplified lumped-circuit simulation based on the measured dc characteristics still provides valuable information. The simplified simulations are very useful to guide the first-round design of the device structure.

A current-voltage curve obtained from a good RTD [1] is plotted in Fig. 1. A simplified equivalent circuit model for a single RTD is illustrated in Fig. 2(a), where a capacitance ($C$) in shunt with a conductance ($G$) is in series with a parasitic series resistance ($R_{se}$). A "quantum-well inductance" due to the effect of quasibound-state lifetime was included in the equivalent circuit model in [3]. It is neglected in our analysis. In the millimeter-wave frequencies, this effect is not important. Instead, transit time effects are more relevant. They make about 13% correction on the device impedance as will be shown later.

From the data of the quoted RTD device, the series resistance, which is determined by the ohmic contact, the undepleted epilayer resistance, and the spreading resistance, is calculated to be about 15 Ω [1]. The corresponding specific series resistance is $1.9 \times 10^{-6}$ Ω-cm$^2$. In calculating this, the specific contact resistance of $10^{-6}$ Ω-cm$^2$ is assumed and the n-type doping concentration in the epilayers is $2 \times 10^{17}$ cm$^{-3}$. When neglecting transit time effects, the small-signal conductance is estimated to be $-13$ mS, or $-1$ mS/$\mu$m$^2$, if the diode is biased at 0.95 V. The capacitance is contributed by the depletion length in the anode, the double-barrier quantum well length, and the accumulation layer length in the cathode. As a result, the total capacitance is about 0.02 pF, (which is mainly due to a depletion layer thickness of 700 Å,) equivalent to a capacitance per unit area of 1.6 fF/$\mu$m$^2$. For simplicity, we will assume that diode capacitance is approximately a constant, even under a large RF signal operation. When two or more RTD's are integrated in series, heavily doped spacer layers can be used to separate the double-barrier quantum wells (added with their associated depletion layers) so that the diodes in the series-integrated structure are decoupled from each other quantum mechanically by negligible resistance [10].

Based on these considerations, a proposed layer structure for a three-RTD device is shown in Fig. 3. It is assumed that the series-integrated device is grown on a 70-nm-thick epitaxial layer doped to $2 \times 10^{17}$ cm$^{-3}$. Practically, a thin buffer layer may be needed between the heavily-doped substrate and the very first epitaxial layer. A $2 \times 10^{18}$ cm$^{-3}$ doped spacer layer with a 500 Å thickness is sandwiched between RTD's. The epilayer thickness of each RTD outside the barriers has been reduced to zero at cathode side and to 70 nm at anode side to keep the capacitance and the series resistance of each diode small enough. The transit time effects will be considered later

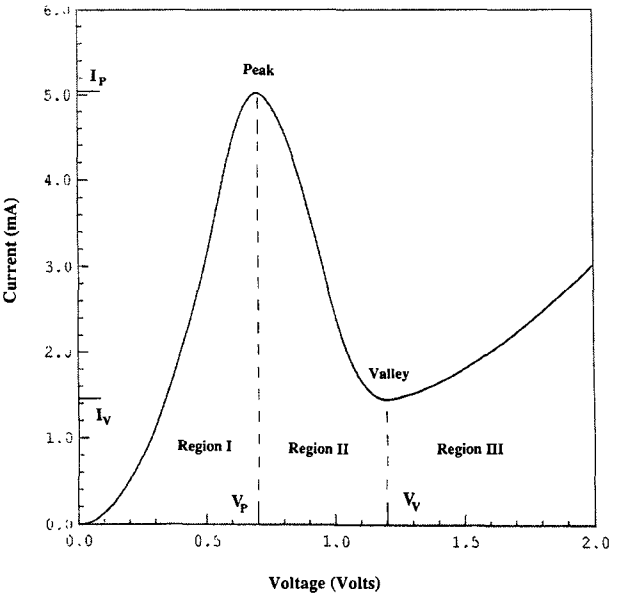


Fig. 1. Current-voltage characteristic of a GaAs/AlAs double-barrier quantum-well RTD fabricated by Brown *et al.* [1]. $I_p$ and $I_v$ are the peak and the valley currents, respectively. $V_p$ and $V_v$ are the peak and the valley voltages, respectively. Region I and region III have positive differential resistance, while region II has negative differential resistance.

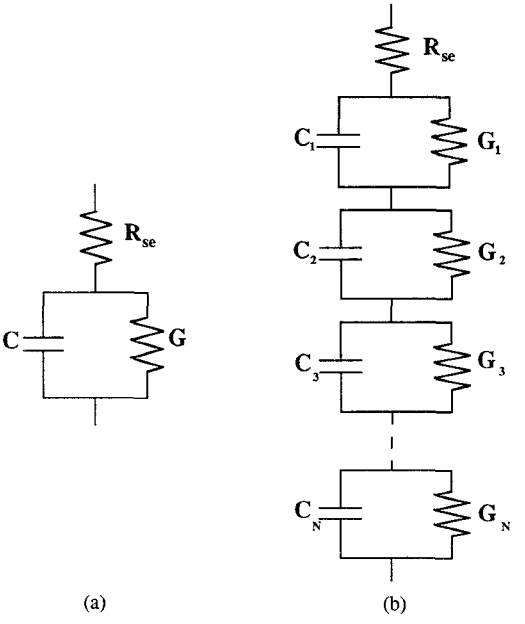


Fig. 2. Equivalent circuit model for (a) a single RTD, and (b) a series-integrated RTD. $R_{se}$ is the total series resistance. $C$ and $G$ are the capacitance and the conductance, respectively.

to further justify the choice of the 70-nm drift region. Consequently, the capacitance per unit area for each unit RTD is still about 1.6 fF/$\mu$m$^2$. The specific resistivity due to one spacer layer is estimated as $8 \times 10^{-9}$ Ω-cm$^2$, which is negligible. The total series resistance for a single diode and a series-integrated diode is basically the same, because it is dominated by the supporting substrate layer and the ohmic contact. The average reduced series resistance per unit diode is a very important factor to the device's RF performance as more diodes are integrated in

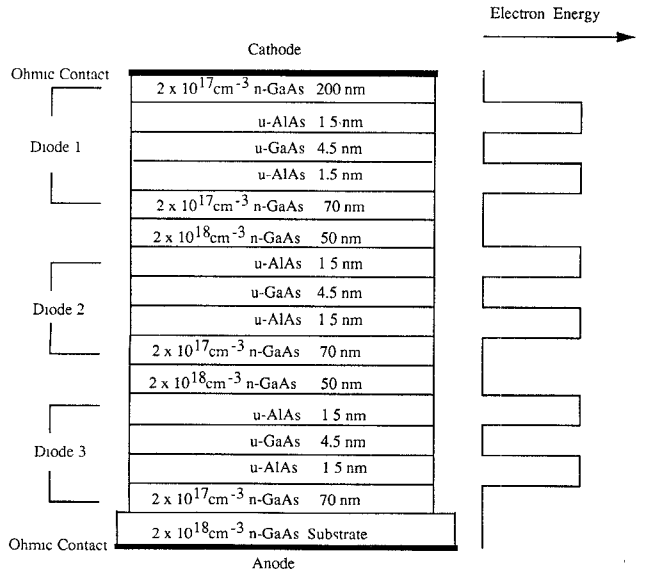


Fig. 3. Cross section layers of a proposed device structure with three RTD's integrated in series. The thickness and the doping concentration of each layer are indicated. *u* means undoped. The conduction band diagram at equilibrium is also shown.

series. It is straightforward to extend the device structure in Fig. 3 to a *n*-RTD device design. The simplified equivalent circuit model of a series-integrated RTD is shown in Fig. 2(b).

## III. Quantitative Formulations for Analysis and Simulation

The higher cutoff frequency of the RTD when compared with the tunnel diode is due to the compatibility of adding a depletion region to the intrinsic RTD structure to reduce the effective capacitance. The length of the depletion region is limited by carrier transit time effects. Although transit time effects are not crucial in the series-integrated oscillatory scheme, they are not negligible for RTD's operated at millimeter-wave frequencies. For a quantitative analysis, transit time effects should be properly treated.

The analysis by Vorontsov and Polyakov did not consider transit time effects [8]. In their analysis, the total current ($I_{\text{tot}}$) of each diode is composed of a displacement current due to junction capacitance and a conduction current, i.e.,

$$I_{\text{tot}}(t) = C\frac{dV(t)}{dt} + I_c(V(t)) \tag{1}$$

where $C = C(V)$ is the junction capacitance from the depletion approximation, and $I_c(V)$ is from the diode dc current-voltage characteristic. Due to transit time effects, the conduction current is no longer a spatial constant along the current flowing direction. Thus, a necessary modification of (1) is to replace the conduction current of a tunnel diode by an appropriately averaged conduction current in a RTD including its drift region. Based on the general current conduction equation and the continuity equation, the induced current ($I^{\text{ind}}$) usually defined as follows provides the correct expression for the averaged conduction current [5], [12].

$$I^{\text{ind}}(t) = \frac{L}{L+W} I^{\text{inj}}(t) + \frac{1}{L+W}\int_0^W \int_0^\infty v(\tau)\, g(x,\tau)\, I^{\text{inj}}(t-\tau)\, d\tau\, dx \tag{2}$$

where $I^{\text{inj}}$ is the conduction current of the injector which is the intrinsic RTD of length $L$, $W$ is the drift region length, $v(t)$ is the average carrier transient velocity after injection, and $g(x, t)$ is the Gaussian profile function describing the carrier transient diffusion and drift motion after injection [5], [12]. Note that the consideration of transit time effects demands a detailed treatment of the carrier motion in the short drift region. $I^{\text{ind}}(t)$ is essentially a weighted average of $I^{\text{inj}}(t)$ over the transit time. Since we neglect the quantum-well inductance, the injector current ($I^{\text{inj}}$) is an explicit function of the injector voltage ($V^{\text{inj}}$). It is simply given by

$$I^{\text{inj}}(t) = I(V^{\text{inj}}(t)). \tag{3}$$

The voltage $V(t)$ across the diode, which is the sum of the injector voltage and the voltage across the drift region including carrier space charge effects, can be expressed as [5], [12]

$$V(t) = V^{\text{inj}}(t) + \frac{W}{L} V^{\text{inj}}(t) - \frac{qN_D W^2}{2\epsilon} + \frac{1}{\epsilon A}\int_0^W \int_0^x \int_0^\infty g(x',\tau)\, I^{\text{inj}}(t-\tau)\, d\tau\, dx'\, dx \tag{4}$$

where $q$ is the electron charge, $\epsilon$ is the permittivity, $N_D$ is the doping concentration in the drift region, and $A$ is the area of the diode.

For lumped-circuit analysis as in [8], the use of an explicit diode $I$–$V$ characteristic as in (1) is always implied. When transit time effects are considered, $I_c(V(t))$ in (1) should be replaced by $I^{\text{ind}}(t)$ of (2) for the circuit analysis. In this situation, the induced current depends not only on the instantaneous voltage $V(t)$, but also on the previous voltage $V(t' < t)$ up to about an interval of the transit time. The functional relationship between $I^{\text{ind}}(t)$ and $V(t)$ is therefore very complicated. The relationship is mainly determined through $V^{\text{inj}}(t)$, which is only a portion of $V(t)$. It should be pointed out that carrier space charge effects further complicate the dependence of $V^{\text{inj}}(t)$ on $V(t)$ as shown in (4). Apparently, the circuit analysis becomes tremendously involved because of transit time effects. In this section, we will present the procedure of a detailed circuit analysis for the proposed generic device structure using (2) and (4) only in the case of a sinusoidal steady state, in which the time dependence becomes simple enough so that the integral in (2) and (4) can be reduced to a simpler form [12]. However, it can be shown that the

arguments used for transient analysis in [8] are still essentially valid even if transit time effects are considered.

The induced current $I^{ind}(t)$ is an averaged $I^{inj}(t)$ over the transit time, so the effective NDR determined by (2) and (4) is usually smaller than that obtained directly from the dc $I$–$V$ characteristics. This is simply a smearing-out effect of the averaging. Therefore, the characteristic time of the dc instability obtained by using static dc $I$–$V$ characteristics without considering transit time effects as done in [8] is in general an overestimate. The turn-on time of a dc power supply can thus be conservatively determined by the dc $I$–$V$ curve. We should point out that there is an additional capacitive current in $I^{ind}(t)$ due to carrier space charge effects, but it is not significant when evaluated numerically. Since an optimized length of the drift region corresponds to a transit angle in the range of $40° - 90°$ for RTD's [5], transit time effects are significant, but should not be drastic. This expectation will be further confirmed by our steady-state sinusoidal analysis results reported in next section. Because simple lumped-circuit calculations can still provide meaningful quantitative results, we will first outline our procedure in terms of a lumped-circuit approach, which is much easier, and then provide the modifications to include transit time effects in detail.

When a $n$-RTD device is in operation, $n$ nonlinear coupled differential equations can be written as

$$C\frac{dV_i(t)}{dt} = \frac{V_{tot}(t) - \sum_{i=1}^{n} V_i(t)}{R_{se}} - I_i(V_i(t))$$
$$i = 1, 2, \cdots, n \qquad (5)$$

where $I_i(V_i)$ is the current-voltage characteristic of the $i$th diode, $R_{se}$ is the series resistance at the ends of the series-integrated device, and $V_{tot}$ is the total voltage across the device. The total voltage is given as the sum of dc and RF voltages, so (5) can be solved numerically to find out the steady-state voltage across each individual diode in time domain. The harmonics of the RF voltage are not included in $V_{tot}$ in our simulations, because the embedding circuit impedances at all harmonic frequencies are assumed to be zero as is commonly done in nonlinear circuit designs. On the other hand, the harmonics of the total current are allowed.

Without transit time effects, numerical simulations can be carried out by solving (5). The conduction current across each individual RTD in (5) is simply the experimental $I$–$V$ curve of Fig. 1. When transit time effects are included, the relationship between the conduction current and the voltage across the single diode is no longer that simple. In this case, it is convenient to use $V^{inj}$ for each RTD as a controlling parameter in simulations. We assume a sinusoidal form as

$$V^{inj}(t) = V_{dc}^{inj} + V_{RF}^{inj}\cos(\omega t). \qquad (6)$$

An approximate $I^{inj}(V^{inj})$ function was obtained in [5] by using only one scaling parameter. In this work, a more accurate $I^{inj}(V^{inj})$ function is obtained by calculating (4) at three most critical points, i.e., the peak and the valley voltages, as well as the middle voltage in between. It should be pointed out that the conduction current in (2) expressed in terms of Gaussian profile function is not exact but a good approximation. This can be understood by checking that the current continuity requirement is not strictly satisfied by the adopted form of (2). However, it seems to us that no simple analytical expression can be found to further improve the accuracy of the description of the carrier transport. Therefore, we still adopt Gaussian distribution form shown in (3) of [5] in this work. Indeed, all the primary features of the nonstationary carrier transport, i.e., velocity overshoot and diffusion, are contained in this form. The initial velocity of the injected carriers is around $7 \times 10^7$ cm/s due to the high electric field at the front of the drift region. This high initial velocity will decay to a steady-state value of $6 \times 10^6$ cm/s with a decay time of $8 \times 10^{-14}$ s [5]. The carrier velocity equation, $v(t)$, as a function of time is basically the same as (6) in [5]. The diffusivity is set at 15 $cm^2/s$, assuming that the diffusivity transient is not significant due to the high electrical field across the diode. The injector length ($L$) and the drift region length ($W$) are 75 Å and 700 Å, respectively. The doping concentration ($N_D$) in the drift region is $2 \times 10^{17}$ $cm^{-3}$ as shown in Fig. 3.

The dc bias condition and the RF voltage should remain the same for cases with and without transit time effects included in the depletion region in order to compare the results. The dc bias on each diode is set at center voltage point of the NDR regime of the measured diode $I$–$V$ curve when transit time effects are excluded. When transit time effects are considered, this is equivalent to setting the dc bias at center voltage point of the NDR regime of the injector $I$–$V$ curve. In order to facilitate comparison, when transit time effects are included, the RF voltage amplitude at the injector is determined in such a way that the RF voltage amplitude across the diode should match to that obtained by excluding transit time effects. In brief, for simulations including transit time effects, we start from (6), calculating $I^{ind}$ in (2) to replace $I_c$ in (1) to obtain $I_{tot}(t)$ and calculating $V(t)$ in (4) to be used for each $V_i(t)$ in (5). In this case, $V_{tot}(t)$ thus obtained is not exactly a dc plus a fundamental. Therefore, Fourier components are taken for both $I_{tot}(t)$ and $V_{tot}(t)$.

## IV. Simulation Results

Runge–Kutta method is employed to solve the nonlinear coupled differential equations. The number of the points required for a convergent solution depends upon diode capacitance, oscillation frequency, and RF voltage amplitude. The numerical solutions are obtained in time domain when a steady state is reached. An algorithm of Fast Fourier transformation (FFT) is then employed to calculate the RF parameters in frequency domain.

The experimental diode $I$–$V$ curve in Fig. 1, the re-

lated dc parameters from Section II, and the reported data in [1] are used in our simulations. Note that current densities are actually used in our simulations and total device area is to be determined. Both two-RTD and three-RTD devices are simulated numerically at 100 GHz. The total dc bias voltage is set in such a way that dc operating point for each individual diode is located approximately at center voltage point of NDR regime, which has a value of 0.95 V. The dc bias voltages are therefore set at 1.95 V for a two-RTD device, and 2.9 V for a three-RTD device, where a voltage drop across series resistance is approximately 0.5 V. We find, as expected, that a stable oscillation can occur only if RF voltage amplitude is greater than a cutoff value ($V_c$). Below $V_c$ a steady state generating a negative RF conductance can not be reached. The dc operating point of each individual diode will eventually move back to a PDR regime due to the instability mentioned previously. Table I, which lists RF cutoff voltages obtained from simulation results, indicates that RF cutoff voltage is about 39% of dc bias voltage ($V_{dc}$). The maximum output power and the best dc-to-RF conversion efficiency are evaluated at RF cutoff voltage. The results are also summarized in Table I.

Because a full-scale simulation of the whole integrated structure including transit time effects is very involved, we adopt the approach described in Section III. We have not computed RF cutoff voltage ($V_c$) under the consideration of transit time effects. We expect that $V_c$ should be slightly smaller if transit time effects are included. The results for $V_c$ listed in Table I should provide a good approximation. The transit time effects are evaluated by using (2) and (4) for a single RTD for a number of RF voltages above $V_c$. The admittances per unit area thus obtained are used to calculate the corresponding power and efficiency of the total integrated device. The RF voltage waveforms are sinusoidal in our simulations. For each given value of $V_{RF}$ simulated without transit time effects, a corresponding $V_{RF}^{inj}$ is guessed and iterated until we find the same $V_{RF}$ value which is obtained from the fundamental component of $V(t)$ in (4). This simplification still demands a laborious effort to carry out calculations. When excluding transit time effects, the minimum RF voltage amplitude across a RTD to stabilize the series-integrated RTD oscillator is found to be 0.38 V, if the dc bias at each diode is set at 0.95 V. This is equivalent to a RF voltage amplitude of 0.038 V with a dc voltage drop of 0.154 V at injector when transit time effects are included.

When transit time effects are included in the simulation, the device's overall RF performance degrades because of the reduced negative conductance. The total output power and the dc-to-RF conversion efficiency of a two-RTD device versus RF voltage amplitude are plotted in Fig. 4 for both with and without transit time effects, assuming a 5-Ω output load is matched at 100 GHz. As shown, the efficiency, which is proportional to the RF conductance, drops about 13% from the best value of 8.6% to 7.4% because of transit time effects. The total output power, which is approximately proportional to the RF conductance square, drops about 25% from the maximum value of 3.84 mW to 2.86 mW.

TABLE I
RF CUTOFF VOLTAGES AND THE BEST PERFORMANCE DATA OF TWO-RTD AND THREE-RTD DEVICES

| Diode Numbers | DC Bias Voltage (V) | RF Cutoff Voltage (V) | Total Power (mW) | Efficiency (%) |
|---|---|---|---|---|
| 2 | 1.95 | 0.76 | 3.84 | 8.6 |
| 3 | 2.90 | 1.14 | 11.17 | 9.9 |

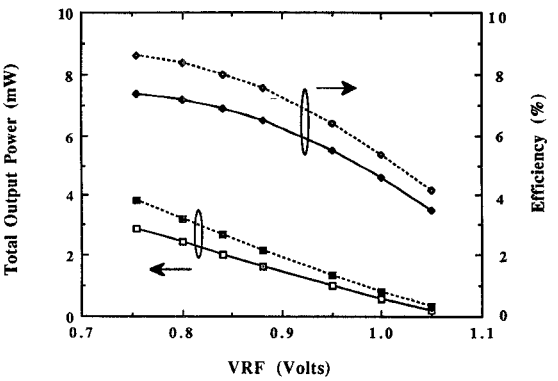


Fig. 4. Total output power and dc-to-RF conversion efficiency versus RF voltage amplitude for a two-RTD device matched to a 5-Ω load at 100 GHz. Solid lines include transit time effects, while dotted lines do not.

Based on the analysis and simulation procedures outlined in Section III, our results for the best dc-to-RF conversion efficiency and the maximum total output power of the proposed integration structure versus the number of the integrated RTD's are plotted in Fig. 5. The corresponding total device area ranges from 80 $\mu m^2$ for a two-RTD device to 630 $\mu m^2$ for a ten-RTD one. As shown in Fig. 5, the efficiency of the proposed integration structure can be as high as 11.5% using device parameters from available experimental data. The transit time effects degrade the efficiency from 11.5% to 10%. This degradation is understandable because transit time effects usually smear out the effective NDR to some extent. It should be pointed out that the degradation is not drastic as expected earlier due to the small transit angle involved. The total output power of the proposed integration structure is roughly proportional to the square of the integrated diode numbers as shown in [9]. It can be as high as about 0.165 W when ten RTD's as structured in Fig. 3 are integrated. The transit time effects degrade the power from 0.165 W to 0.12 W, i.e., a degradation of about 27%. Estimations in [8] have shown that with a 20% spread of peak currents it is possible to draw over 75% of the maximum possible power generated from the series-connected identical diodes. If a 20% spread of peak currents is assumed here, then the maximum stable output power is around 0.1 W with the best associated efficiency of about 8% for a ten-RTD device. Each RTD is biased at 0.95 V, thus a 9.55-V voltage shock wave is required to initiate an oscillation. As the number of the integrated RTD's is increased, the best efficiency is improved due to the virtually unchanged

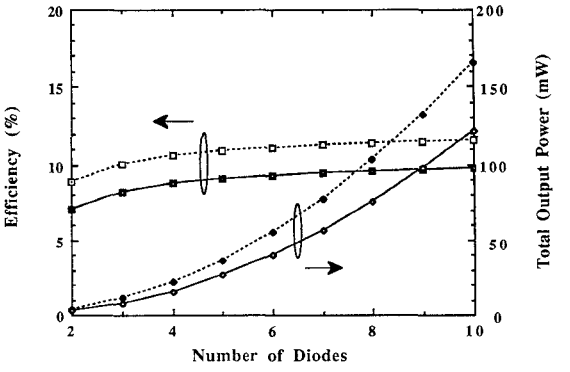


Fig. 5. The best dc-to-RF conversion efficiency and the maximum total output power from the series-integrated resonant tunneling diodes versus the number of the integrated diodes. A 5-Ω output load is assumed to be matched at 100 GHz. Solid lines include transit time effects, while dotted lines do not.

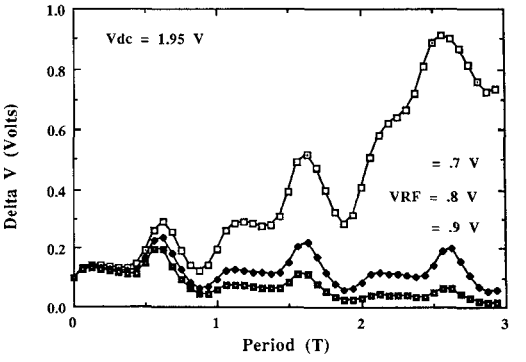


Fig. 6. Voltage deviation ($\Delta V$) between two RTD's versus time at three different RF voltage amplitudes. The initial voltage deviation is 0.1 V. The curve corresponding to $V_{RF} = 0.7$ V shows RF instability.

total series resistance, which is dominated by the substrate supporting layer and the ohmic contact.

It has been mentioned that RF voltage amplitude determines the existence as well as the magnitude of the total negative RF conductance of the series-integrated RTD's. A too small RF voltage amplitude cannot maintain a negative conductance due to the instability explained earlier. In our simulations the RF voltage amplitude plays an important role in controlling voltage convergence rate when solving (5) numerically. As an example, a two-RTD device is selected to demonstrate transient behavior in simulation. The total dc bias voltage is set at 1.95 V, and the initial voltage deviation between two diodes is set at a value of 0.1 V. The simulation results are illustrated in Fig. 6, where three different RF voltage amplitudes are used. In the case of $V_{RF} = 0.7$ V, which is less than the cutoff value ($V_c = 0.76$ V), the voltage deviation grows with time. Eventually, dc operating points will move out of NDR regime of diode $I$–$V$ curve, causing no oscillation. However, in the case of $V_{RF} = 0.8$ V, which is a little greater than $V_c$, the voltage deviation decays with time. This produces a stabilized oscillation mode. If RF voltage amplitude is further increased to 0.9 V, a faster convergence is observed. This shows that the voltage convergence rate is a strong function of RF voltage amplitude.

A related result due to the dc instability is that the negative conductance of the series-integrated RTD should exist only in a band of frequency. Its lower frequency limit ($f_L$) is approximately $|G_n|/(2\pi C\gamma)$, where $G_n$ is the negative conductance of a single RTD, $C$ is the associated capacitance, and $\gamma$ is an empirical parameter related to the device transient behavior. It is difficult to characterize the device transient behavior in a general way. As shown in Fig. 6, it depends on the initial voltage deviation and the RF voltage amplitude. For the device parameters used in this work, $\gamma$ and $f_L$ are in the order of 10 and 10 GHz, respectively.

## V. Conclusion

In summary, the double-barrier quantum-well RTD shows great potential for millimeter-wave source. In order to increase the total output power as well as to remove the low-frequency instability of a single RTD, a series-integrated device structure, which can be grown by the advanced MBE technology, is proposed. The minimum slope of the excitation pulse leading edge required to initiate an oscillation is estimated to be $5 \times 10^{11}$ V/s. This requirement is entirely feasible due to the recent demonstration of NLTL for picosecond shock wave generation.

The low-frequency spurious oscillations associated with the single RTD are frequently observed, when it is biased at NDR regime of its $I$–$V$ curve. Unlike IMPATT or Gunn diodes, the RTD bears NDR almost from dc to millimeter-wave frequencies. This makes the RTD quite difficult to use at high frequencies. The problem of low-frequency spurious oscillations will no longer exist when the series-integrated device is driven into the oscillation mode, because the stable self-oscillation occurs only within a certain frequency band.

Simulations with and without transit time effects included in the depletion region are performed at 100 GHz. We find that the negative conductance and the dc-to-RF conversion efficiency degrade about 13%, while the total output power degrades about 25%, when transit time effects are included. This relatively small degradation is because the injection phase angle of a RTD is about 270° and the drift angle is usually only 90° or less, thus causing no drastic effect. The total output power of 0.1 W with the associated dc-to-RF conversion efficiency of 8% from a ten-RTD device matched to a 5-Ω output load is obtained at 100 GHz, if a 20% spread of peak currents is assumed. When more RTD's are integrated, the efficiency can be enhanced due to the relatively unchanged total series resistance. The processing uniformity and the thermal consideration will probably limit the number of the integrated diodes. The RTD device structure and the doping concentration in the epilayers are not optimized in this work. It is possible to further improve the RF performance of the series-integrated RTD's. Unlike RTD's, the efficiency of conventional IMPATT diodes is bound to drop quickly beyond 100 GHz, because it is difficult to localize the ionization injection. The noise performance of RTD's is also expected to be substantially better than IMPATT diodes due to the less noisy tunneling process.

## REFERENCES


[1] E. R. Brown, T. C. L. C. Sollner, W. D. Goodhue, and C. D. Parker, "Millimeter-band oscillations based on resonant tunneling in a double-barrier diode at room temperature," *Appl. Phys. Lett.*, vol. 50, pp. 83–85, Jan. 1987.

[2] R. C. Potter, A. A. Lakhani, D. Beyea, H. Hier, E. Hempfling, and A. Fathimulla, "Three-dimensional integration of resonant tunneling structures for signal processing and three-state logic," *Appl. Phys. Lett.*, vol. 52, pp. 2163–2164, June 1988.

[3] E. R. Brown, T. C. L. G. Sollner, C. D. Parker, W. D. Goodhue, and C. L. Chen, "Oscillations up to 420 GHz in GaAs/AlAs resonant tunneling diodes," *Appl. Phys. Lett.*, vol. 55, pp. 1777–1779, Oct. 1989.

[4] V. P. Kesan, D. P. Neikirk, B. G. Streetman, and P. A. Blakey, "A new transit-time device using quantum-well injection," *IEEE Electron Device Lett.*, vol. EDL-8, pp. 129–131, Apr. 1987.

[5] I. Song and D. S. Pan, "Analysis and simulation of the quantum well injection transit time diode," *IEEE Trans. Electron Devices*, vol. 35, pp. 2315–2322, Dec. 1988.

[6] V. P. Kesan, A. Mortazawi, D. R. Miller, V. K. Reddy, D. P. Neikirk, and T. Itoh, "Microwave and millimeter-wave QWITT diode oscillators," *IEEE Trans. Microwave Theory Tech.*, vol. 37, pp. 1933–1941, Dec. 1989.

[7] H. Grönqvist, A. Rydberg, H. Hjelmgren, H. Zirath, E. Kollerg, J. Söderström, and T. Anderson, "A millimeter wave quantum well diode oscillator," in *Proc. 18th European Microwave Conf.*, Stockholm, Sweden, Sept. 1988, pp. 370–375.

[8] Y. I. Vorontsov and I. V. Polyakov, "Study of oscillatory processes in circuits with several series-connected tunnel diodes," *Radio Eng. Electron. Phys.*, vol. 10, pp. 758–763, May 1965.

[9] D. S. Pan, C. C. Yang, C. Jou, and B. Jogai, "Multi-layered heterojunction structure for millimeter wave sources," *The Physics of Submicron Structures*, H. L. Grubin, K. Hess, G. J. Iafrate, and D. K. Ferry, Eds. New York and London: Plenum, 1984, p. 327.

[10] E. Wolak, B. G. Park, K. L. Lear, and J. S. Harris, Jr., "Variation of the spacer layer between two resonant tunneling diodes," *Appl. Phys. Lett.*, vol. 55, pp. 1871–1873, Oct. 1989.

[11] C. J. Madden, R. A. Marsland, M. J. M. Rodwell, D. M. Bloom, and Y. C. Pao, "Hyperabrupt-doped GaAs nonlinear transmission line for picosecond shock-wave generation," *Appl. Phys. Lett.*, vol. 54, pp. 1019–1021, Mar. 1989.

[12] I. Song and D. S. Pan, "A generalized analytical model for the quantum well injection transit time diode," *IEEE Trans. Electron Devices*, vol. 38, pp. 14–22, Jan. 1991.


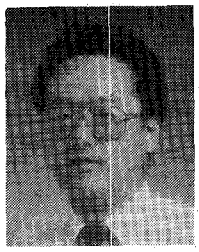

**Cheng Chih Yang** (M'87–S'87–M'89) received the B.S. degree from National Cheng Kung University, Tainan, Taiwan, Republic of China, and the M.S., Engineer, and Ph.D. degrees in electrical engineering from the University of California, Los Angeles.

He then began his career with Commodore Inc., Costa Mesa, CA, where he was responsible for SPICE modeling and CMOS circuit designs. In 1984, he joined Electronic Systems Group of TRW Inc., Redondo Beach, CA, where he has been involved in microwave and millimeter-wave circuits and subsystems designs. Currently, he is interested in the development of millimeter-wave monolithic integrated circuits and subsystems for communication system insertion.

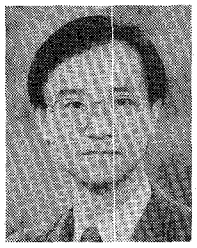

**Dee-Son Pan** (M'79–M'89) received the B.S. degree in physics from Tsing-Hwa University, Taiwan, China in 1971, and the Ph.D. degree in physics from the California Institute of Technology in 1978.

He joined the faculty of the Electrical Engineering Department at UCLA as an Assistant Professor in 1977, where he is currently an Associate Professor. His current research interests are device modeling, semiconductor physics and theoretical exploration of new devices.